

Synthesis, Characterization and Cytotoxicity Evaluation on Monocytic Cell Line THP1 of Ru(II) Complexes with 1, 2-Disubstituted Benzimidazoles

Ashok Kumar Singh^{1*}, Snehlata Katheria¹, Asif Jafri² and Md. Arshad²

¹Department of Chemistry, University of Lucknow, Lucknow - 226007, INDIA

²Department of Zoology, University of Lucknow, Lucknow - 226007, INDIA

* Correspondence: E-mail: singhaks3@rediffmail.com

DOI: <http://dx.doi.org/10.33980/jbcc.2019.v05i01.021>

(Received 17 Apr, 2019; Accepted 26 May, 2019; Published 07 Jun, 2019)

ABSTRACT: A series of mononuclear ruthenium complexes containing monodentate ligand Benzimidazole have been synthesized and their biological properties have been examined. The ruthenium(II) complexes with substituted benzimidazole were prepared of the general formulae $[\text{RuCl}_3(\text{HL})_3\text{H}_2\text{O}]$ (HL1 = 2-(3-bromopropyl)-1*H*-benzo[*d*]imidazole; HL2 = 2-(4-chlorophenyl)-1*H*-benzo[*d*]imidazole; HL3 = 4-(1*H*-benzo[*d*]imidazole-2-yl)aniline; HL4 = 2-(4-nitrophenyl)-1*H*-benzo[*d*]imidazole; HL5 = (1*H*-benzo[*d*]imidazole-2-yl)methanethiole). The complexes were characterized by conductivity measurements, elemental analysis, infrared, electronic, ¹H and ¹³C-NMR and Mass spectral studies. The complexes were optimized by using Gaussion-09. The biological activities of ruthenium complexes were evaluated on human acute monocytic leukemia cells (THP-1) by MTT cell viability assay, ROS generation and nuclear apoptosis analysis. The MTT assay revealed that these synthesized complexes, significantly reduces the viability of THP-1 cells, in a concentration-dependent manner. Interestingly, these compounds also produce the intracellular reactive oxygen species (ROS) as well as induce the fragmented and condensed nuclei, suggest cell death by an apoptotic process. Biological activity data evidently supported that these complexes induce the apoptotic cell death in THP-1 cells.

Keywords: Apoptotic cells; 1, 2-Disubstituted Benzimidazoles; Nuclear Fragmentation; Optimized Geometry; Ru(II) complexes and ROS Generation.

INTRODUCTION: The medicinal value of cis-Platin has led to the discovery of alternative metal complexes with better medicinal properties.¹ Ruthenium based metal complexes have novel anticancer properties.² Ruthenium complexes with ligands containing groups as amines, imines and imidazoles such as [ImH][trans-Ru(III)Cl₄(dmsO-S)(Im)](NAMI-A; Im = Imidazole, dmsO = dimethylsulfoxide) and [IndH][trans-Ru(III)Cl₄(Ind)₂] (KP1019; Ind = indazole), have successfully completed phase-1 clinical trials and are scheduled to enter phase 2 trials in the near future.^{14,3,4} In addition, benzimidazole derivatives show significant anti-inflammatory, antioxidant, gastroprotective and anti-parasitic activities. Therefore, large number of its metal complexes has been synthesized and applied in urea recognition, DNA binding, catalysis and chemical sensors in biological systems.^{5,6} With bis-benzimidazole derivatives, ruthenium compounds exhibit powerful cytotoxicity against ovarian carcinoma cells, which creates the underlying mechanism

of anticancer functions.^{7,8} Ruthenium is an alternative to platinum, because of accessible oxidation states and less toxic than platinum counterpart, which makes them significant for anticancer activities under physiological conditions.^{9,10} This is due to the ability of ruthenium to mimic iron in the binding to biological molecules, such as albumin and transferrin, although platinum drugs can also bind to the proteins.¹¹ Since rapidly dividing cells, such as cancerous cells, more demand for iron, transferrin receptors are over-expressed, so that ruthenium-based medicines can be delivered more effectively to cancerous cells.¹² Furthermore, activation by "reduction" mechanisms may be responsible for toxicity of some ruthenium compounds.¹³ In the last two decades, a new approach to the treatment of cancer, known as Targeted Medicine and Targeting Cellular Signaling Path of Cancer Cells, starts producing highly effective cancer treatment with very little serious side effects.^{15, 16} Some of them, e.g. Imatinib mesylate and Erlotinib hydrochloride have

established such capability that their approval procedures were tracked rapidly by the American Food and Drug Administration.¹⁷ After all, targeted therapy can become the mainstream in the form of the first line therapeutic options, which can replace existing classical anticancer drugs such as 5-fluorouracil and cisplatin.¹⁸ Therefore, it is worthwhile to consider the current methods being used to develop Ruthenium-based anticancer drugs.¹⁹ In this respect, we have synthesised ruthenium benzimidazole complexes and assessed their Antiproliferative, intracellular ROS and nuclear fragmentation studies on THP-1 Cells of Human acute monocytic leukemia.

MATERIALS AND METHODS:

Chemicals and reagents: All reagents used were of analytical grade. The Chemical used for synthesis were obtained from Sigma Aldrich, Himedia, and Merck was used without further purification. Hydrated $\text{RuCl}_3 \cdot 3\text{H}_2\text{O}$ was purchased from Sigma Aldrich, Himedia and Merck. The solvents were purified according to standard procedure.²⁰ According to the reported method; the method of synthesis of ligands and metal complexes was demonstrated.²¹

Physical measurement: The microanalysis of carbon, hydrogen, and nitrogen of the compounds were carried out on a Carlo-Erba analyser. The FT-IR spectra (KBr) were recorded on a Nicolet 4000D spectrophotometer. Molar conductivity measurements were made on Microprocessor Based conductivity/TDS Meter ESICO, Model-1601 Cell Const $K=1.106$. NMR spectra were recorded (DMSO-*d*₆) on Bruker-300MHz spectrometer using TMS as the internal standard. Electronic spectra were recorded on a Labtronics LT 2900 spectrophotometer.

In vitro cytotoxicity activity studies:

Cell line and culture: The human monocytic leukemia cell line (THP-1) was obtained from the cell repository of National Centre for Cell Sciences (NCCS), Pune, India. The cells were maintained in RPMI culture media supplemented with 10% fetal bovine serum (FBS), 1% antibiotic solution at 37°C humidified environment and 5% CO_2 .

Cell viability assay by MTT: The THP-1 cells (1×10^4 cells per 100 μL) were seeded in RPMI media in each 96 well culture plate for 24 h as described previously.²² Briefly, the cells were treated for 24h with 10, 20, 40, 80, and 160 μM concentrations of the metal complexes. After incubation period, 20 μL of MTT reagent (5mg/ml stock) was added to each well and kept the plate for 4 h at 37°C. Subsequently, the supernatant

were discarded and 100 μL of DMSO were added to each well to solubilize the obtained formazan crystals. The optical density (OD) was recorded at 540nm with the help of BIORAD microplate reader. The percent cell viability was evaluated with the help of following equation:

$$\text{Cell viability (\%)} = \left[\frac{A_{540} (\text{Treated Cells})}{A_{540} (\text{Control Cells})} \right] \times 100$$

(Where; A= absorbance)

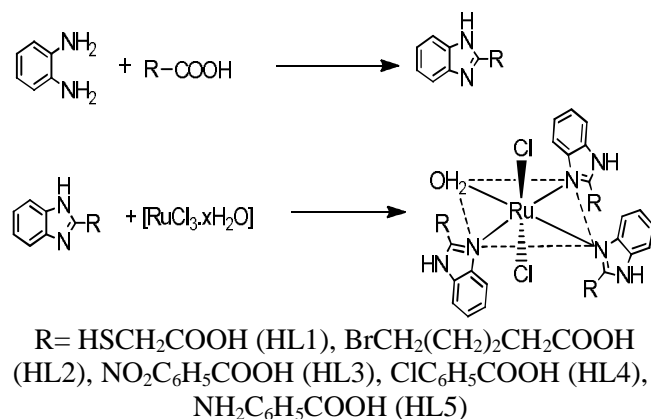
Cellular morphology study by phase contrast microscopy: The cellular morphological alterations in THP-1 cells were observed after treated with different concentrations of the complexes by inverted contrast-phase microscope. Concisely, the THP-1 cells were seeded and treated with different concentrations of the complexes for 24h, as described earlier for MTT assay. Thereafter, the change in cellular morphology was captured by inverted contrast-phase microscope.²²

Intracellular ROS generation in THP-1 cells: The level of intracellular ROS was examined by DCFH-DA (2, 7-dichlorodihydrofluorescein diacetate) staining.²³ Briefly, the THP-1 cells were plated at $1 \times 10^4 / 100\mu\text{L}$ RPMI media in each wells of 96-well culture plate for 24 h, following with the treatment of 40 and 80 μM (effective doses) concentrations of ML4 and ML2 for 12h. Subsequently, the cells were washed with PBS (phosphate buffer saline) and stained with DCFH-DA dye for 20 min at 37°C. The stains were removed from each well followed by gentle washing with PBS to remove excess stain. Finally, the cells were observed and photographed with the help of Nikon inverted fluorescence microscope.

Analysis of nuclear apoptosis in HeLa cells: For the nuclear and chromatin structural changes study, the HeLa cells were seeded in 96 well culture plate and then treated with different doses of complexes at 25, 50 and 100 μM concentrations for 24h.²⁴ Consequently, cells were washed thrice with PBS and fixed in 4% paraformaldehyde (used as a fixative) for 10 min and then permeabilized with permeabilizing buffer (4% paraformaldehyde and 0.5% Triton X-100) and stained with 10mM of DAPI stain. After the staining, cells were examined with the help of inverted fluorescence microscope at the excitation wavelength of 360 nm and an emission wavelength of 454 nm (Nikon ECLIPSE Ti-S, Japan).²⁵ For the quantification analysis of apoptotic cells, test was performed in triplicate for every treatment group and the 100 cells per well were calculated in at least 10 random fields per well, to count the percent apoptotic cells using an inverted

fluorescent microscope (Nikon ECLIPSE Ti-S, Japan).

Statistical analysis: The data of cell viability, nuclear condensation and ROS generation were represented as mean \pm standard error mean (SEM) from at least three independent studies. Determination of difference in between experimental and the control groups were compared during one-way ANOVA followed by Dunnett's multiple range test by Graph Pad prism software (Version 5.01). The *p* value of less than 0.05 was designated to be statistically significant.



Scheme 1: Synthetic route for the synthesis of Ligands and metal complexes.

Synthesis of ligands:

General Procedure for Synthesis of Ligands (HL1-HL5): The substituted benzimidazole ligands were prepared following the reported procedure.²⁶ Further, *o*-phenylenediamine (0.25mmol, 0.265 g) was interreacted with mercaptoacetic acid (0.34mmol, 0.313g), 5-bromovaleric acid (0.34mmol, 0.615g), 4-nitro benzoic acid (0.34mmol, 0.568 g), 4-chlorobenzoic acid (0.34mmol, 0.532g), and 4-aminobenzoic acid (0.34mmol, 0.487g), respectively and heated on water bath at 100°C for 12h. The completion of the reaction was monitored by TLC. After the reaction was completed, the reaction mixture was cooled and basified in a pH of 7-8 using 10% sodium hydroxide solution. The crude substituted benzimidazole was filtered and washed with ice cold water. The crude product was dissolved in 400 ml of boiling water and 2 grams of decolorizing carbon was added and it was digested for 15 minutes. The solution was filtered while hot, cooled the filtrate to about 10°C. The pure product was filtered, washed with 25 ml of cold water and dried at 100°C. The resulting product were obtained as (1*H*-benzo[*d*]imidazole-2-yl)methanethiole (HL1), 2-(3-bromoprpyl)-1*H*-benzo[*d*]imidazole (HL2), 2-(4-nitrophenyl)-1*H*-benzo[*d*]imidazole (HL3), 2-(4-chlorophnyl)-1*H*-benzo[*d*]imidazole] (HL4) and 4-(

1*H*-benzo[*d*]imidazole-2-yl)aniline (HL5) were obtained.²⁷

(1*H*-benzo-*d*]imidazole-2-yl)methanethiol (HL1): Colour: pale yellow solid, % Yield: (42.90, 70g), M.P.-158°C, IR (KBr, ν_{\max} , cm⁻¹):3379 (N-H Str.), 2963(Ar-C-H str.), 2600(S-H Str), 1700(Ar-C-H ben.), 1413(C=N). ¹H NMR (DMSO-*d*₆): δ 7.01-7.51(m, 4H Ar-H), 6.19(s, 1H,C-H), 3.65(s, 1H, OH), 2.2(s 1H, SH). UV-Vis. [λ_{\max} , nm(ϵ ,10³M⁻¹cm⁻¹):230, 250, 290, 350, 380.

2-(4-bromobutyl)-1*H*-benzo[*d*]imidazole (HL2): Colour: Reddish brown solid, % yield: (40.4, 95g), M.P.- 166°C. IR (KBr, ν_{\max} ,cm⁻¹): 3174 (N-H str.), 1527(C=N str.), 2900(ArC-H), 1700 (Ar C=C).¹H NMR (DMSO-*d*₆): δ 6.57-7.90(m, 8H, Ar-H), 6.96(s, 1H, N-H), 2.50-2.54(m, 8H, CH₂);UV-Vis. [λ_{\max} , nm(ϵ , 10³M⁻¹cm⁻¹): 210, 240, 270, 280.

2-(4-nitrophenyl)-1*H*-benzo[*d*]imidazole (HL3): Colour: Brown solid, %yield: (40.50, 95g; M.P.-220°C, IR (KBr, ν_{\max} , cm⁻¹): 3157(N-H str.), 2975(ArC-H), 1350 (NOsymstr), 1427(CNstr)756(CBr), 1700 (C=Cring.str), 1602(N-O asym str), 1539 (C=N str). ¹H NMR (DMSO-*d*₆): δ 7.57-8.22(m, 8H Ar-H), 6.87(S,1H,N-H) UV-Vis.[λ_{\max} , nm(ϵ , 10³M⁻¹cm⁻¹)] 350, 440.

2-(4-chlorophenyl)-1*H*-benzo[*d*]imidazole (HL4): Colour: Black solid, %yield: 39.6, 82g; M.P.-234°C. IR(KBr, ν_{\max} , cm⁻¹); 3165(N-HStr), 3000(Ar C-H), 576(C-Cl), 1525(C=N), 1600(C=C ring system), 1429(C-N str.). ¹H NMR (DMSO-*d*₆): δ 7.52-8.12(m, 8H, Ar-H), 6.80 (s, 1H N-H), UV-Vis. [λ_{\max} , nm(ϵ , 10³M⁻¹cm⁻¹):280, 355, 440.

4-(1*H*-benzo[*d*]imidazol-2-yl) aniline (HL5): Colour: brown, %yield: (42.6, 87g); M.P.: 226°C, IR (KBr, ν_{\max} , cm⁻¹): 3169(NHstr), 1450(C=Nstr), 1650 (ArC=C), 2350 (ArNH(NH₂)), 2900(ArC-H), 1080 (ArC-N). ¹H NMR (DMSO-*d*₆): δ 6.40-7.89(m, 8H Ar-H), 6.40(s, 1H, N-H), 2.50(s, 2H, NH₂) UV-Vis[λ_{\max} , nm(ϵ , 10³M⁻¹cm⁻¹):320,410.

Synthesis of the complexes: Ruthenium(II) complexes were synthesized as reported with some modifications.²⁸ The Ruthenium(III) chloride trihydrate (1mmol, 0.262g) and substituted benzimidazole (3mmol) [(HL1, HL2, HL3, HL4, HL5)] were added in 10ml of acetone and refluxed for 6h under nitrogen atmosphere. The reaction mixture was cooled and filtered, reduced the volume and kept for overnight in defreeze. The solid were filtered, washed with methanol and ether and dried in vacuum. The complexes

were purified by column chromatography over silica gel and methanol as an eluent.

[RuCl₂(HL1)₃(H₂O)](ML1): Colour-dark brown; % Yield-(52,0.50g); M.P-281°C; IR(KBr, ν_{\max} , cm⁻¹): 1328(NH), 2963(Str. NH₂), ¹H NMR (300MHz, δ ppm, DMSO-*d*6): 7.06-8.20(m,4H Ar-H), 4.01(S,1H, NH), 2.40 (2H,CH₂); 2.49(S,1H,SH). ¹³C NMR (300mHZ, δ ppm, DMSO-*d*6): 142.85, 137.95, 132.39, 132.26, 129.94, 129.78, 123.52,116.17, 61.39, 40.33, 40.05, 39.77, 39.49, 39.21, 38.93, 38.65, 32.29, 21.96;UV-Vis. [λ_{\max} , nm(ϵ , 10³M⁻¹cm⁻¹): 220, 255, 280, 310, 440.ESI-MS:[M+1]⁺ 829(830.82)

[RuCl₂ (HL2)₃(H₂O)] (ML2): Colou r- dark green; % Yield-(62,0.63g); M.P - 298°C, IR((KBr, ν_{\max} , cm⁻¹): 1250(NH), 2870(Str. NH₂), ¹H NMR (300MHz, δ ppm, DMSO-*d*6) - 7.26-8.13(m,8H,Ar-H), 6.60(2H, NH), 1.25-3.79(m,16H,CH₂).¹³C NMR(300mHZ, δ ppm DMSO-*d*6): 141.02, 137.59, 132.78, 132.51, 132.29, 132.15, 129.00, 128.83, 123.16, 115.71, 77.64, 77.21, 76.79 ;UV-Vis. [λ_{\max} , nm(ϵ , 10³M⁻¹cm⁻¹):235, 252, 450. ESI-MS:[M+1]⁺ 889(888).

[RuCl₂(HL3)₃(H₂O)](ML3): Colour- dark red; % Yield- (42, 0.50g); M.P-320°C, IR(KBr, ν_{\max} , cm⁻¹):1251(NH), 3200(str. NH₂)¹H NMR (300MHz, δ ppm, DMSO*d*6):7.568.31(16H,ArH),6.60(1H,NH).¹³CNMR(300mHZ, δ ppm DMSO-*d*6):140.85, 137.67, 134.04, 133.78, 132.39, 132.31, 132.18, 130.91, 128.93, 128.77, 128.72, 128.63, 123.76, 123.17, 115.78; UV-Vis. [λ_{\max} , nm(ϵ , 10³M⁻¹cm⁻¹):210, 250, 350, 450. ESI- MS: [M+1]⁺ 906 (906.60).

[RuCl₂(HL4)₃(H₂O)](ML4): Colour- green ; % Yield-(42,0.46g); M.P-308°C;IR(KBr, ν_{\max} ,cm⁻¹): 1416(NH), 3700(Str NH₂),¹H NMR (300MHz, δ ppm, DMSO-*d*6):7.28-8.10(m,ArH),6.80(s,NH),¹³CNMR(300mHZ, δ ppm DMSO-*d*6): 140.89, 137.52, 132.55, 132.27, 132.14, 131.39, 131.34, 131.27, 129.02, 128.85, 128.65, 123.18, 115.67, 77.65, 77.22, 76.80; UV-Vis. [λ_{\max} , nm(ϵ , 10³M⁻¹cm⁻¹): 250, 255, 440, 550. ESI-MS:[M+1]⁺ 816(814.76)

[RuCl₂(HL5)₃(H₂O)](ML5):Colour- brown; % Yield-(38,0.44g);M.P-348°C; IR (KBr, ν_{\max} ,cm⁻¹): 1294 (NH₂), 3300(Str NH₂); ¹H NMR (300MHz, δ ppm, DMSO-*d*6)- δ :8.095 (s, NH), 7.54-7.90 (m, ArH), 2.50 (S,2H,NH₂), 6.42 (S, H, NH), ¹³C NMR(300mHZ, δ ppm DMSO-*d*6): 141.08, 137.64, 134.05, 133.79, 132.30, 132.17, 129.01, 128.91, 128.85, 123.20, 115.74, 77.65, 77.22, 76.80; UV-Vis. [λ_{\max} , nm(ϵ , 10³M⁻¹cm⁻¹):250, 310, 420. ESI-MS: [M+1]⁺788 (784).

RESULTS AND DISCUSSION: The ruthenium trichloride trihydrate reacted with substituted benzimidazoles in 1:3 molar ratios in acetone to yield the title complexes. The proposed molecular formulae for the complexes are in good agreement with the stoichiometry concluded from the analytical data. The complexes ML1, ML2 and ML3 were soluble in common organic solvents such as acetone and alcohol whereas other complexes ML4 and ML5 were sparingly soluble in common organic solvents but soluble in DMF and DMSO. The conductivity measurements were carried out in 10⁻³molL⁻¹ in DMF/DMSO. The molar conductance values were 24–49 Ω^{-1} cm⁻² mol⁻¹. The observed values were not high enough to be characterized as 1:1 electrolytes, but these values fall within the acceptable range for non-electrolytes.²⁸ The higher conductivity values may be due to partial replacement of Chloride in the complex by strong donor solvents.

IR spectra: The IR spectral data of the complexes were compared with those of the free ligands in order to determine the coordination sites. The ligands HL1, HL2, HL3, HL4 and HL5 display ν_{N-H} of substituted benzimidazole at 3379, 3174, 3157, 3165 and 3169 cm⁻¹ respectively.²⁸ The band due to $\nu_{C=N}$ of ligands appeared at 1410-1527 cm⁻¹.The shift in bands, lower or higher, of ν_{N-H} , $\nu_{C=N}$ and $\nu_{C=C}$, respectively in complexes (ML1-ML5), indicate coordination of substituted benzimidazole through tertiary nitrogen of imidazole moiety. Additionally, there is appearance of new band of ν_{Ru-Cl} in the range 480-485cm⁻¹ and ν_{Ru-OH} in the range 746-748cm⁻¹ of ruthenium complexes , suggested the coordination of chloro and water molecules to the metal centre.²⁹

¹H and ¹³C-NMR: The ¹H and ¹³C-NMR spectrum of the ligand and their corresponding ruthenium complexes were recorded in DMSO-*d*6. The electronic environment of aromatic protons for the substituted benzimidazole was found in the range 8.48-6.90 ppm. The singlet proton of NH was occurred in the range 6.87-6.40 in the ligands. The appearance of C-H proton signal at 2.28(s) ppm for one protons corresponds to the HL1 and 2.54-2.28 for eight protons in HL2.The SH proton in HL5 did not appeared due to deuterium exchange. The aromatic protons in ML1-ML5 were downfield shifted and found in the range 8.09-7.26ppm, indicated that the coordination has occurred. The resonance due to CH₂ and NH protons in the corresponding metal complexes shifted by 0.15-0.40 and 0.02-0.40, respectively, which suggested the complexation has occurred. The ¹³C-NMR spectra of the ligand and complexes show signals in the regions that are in agreement with those expected based on the carbon environments. The resonance at 155.34,

134.02, 166.45, 168.56 and 145.37 in the Ligands (HL1-HL5), respectively was assigned to the C=N carbons. The resonance of the CH₂ carbon in LH1 and HL2 ligand occurred near 40.34ppm. The resonance signals due to benzimidazole ring in the complexes occurred in the range 137.52- 115.65ppm. The resonance due to CH₂ carbon in ML1 and ML2 was observed at 61.39 and 76.80, respectively. The resonance signal in the region 142.85 -140.85ppm was observed in all complexes, which indicated the presence of coordinated C=N-M groups.

Electronic spectra: The UV-Vis absorption spectra of ligand and complexes were recorded in CH₃OH at room temperature. The HL1 - HL5 have absorption bands in the range of 210-219 and 350-440 nm, which can be assigned to intra molecular $\pi \rightarrow \pi^*$ transitions. The ML1-ML5 have three absorption bands in the range of 210-280 nm, 310-350 and 420-550nm which can be assigned to $\pi \rightarrow \pi^*$, which can be assigned to intraligand transitions and another absorption bands in the range of 420-550nm, which can be assigned to the spin-allowed metal to ligand charge transfer transitions (MLCT). The absorption band in the range of 420-550nm, which can be assigned to the metal to ligand charge transfer transition (MLCT).

Geometry optimization and structural analyses: The gas phase geometry optimizations for all the complexes were performed by using DFT with the B3LYP exchange correlation functions and using Gaussian-09.³⁰ The full geometry optimisation were performed by using the LANL2DZ basis set for metal ion and 6-31G(d) basis set for C, H, and N atoms. The geometry optimised structures of the complexes show

the similarity with the reported crystal structure of the similar type of the moiety. This shows that the ligand bind in a similar fashion as in the complexes reported. All compounds, the Ru-O bond distances around the metal centre only differ slightly, with bond length ranging 2.229-2.247, confirms the coordination with metal centre. Moreover, the Ru-Cl distance are almost equivalent, 2.584-2.456, which fits within the range.³¹

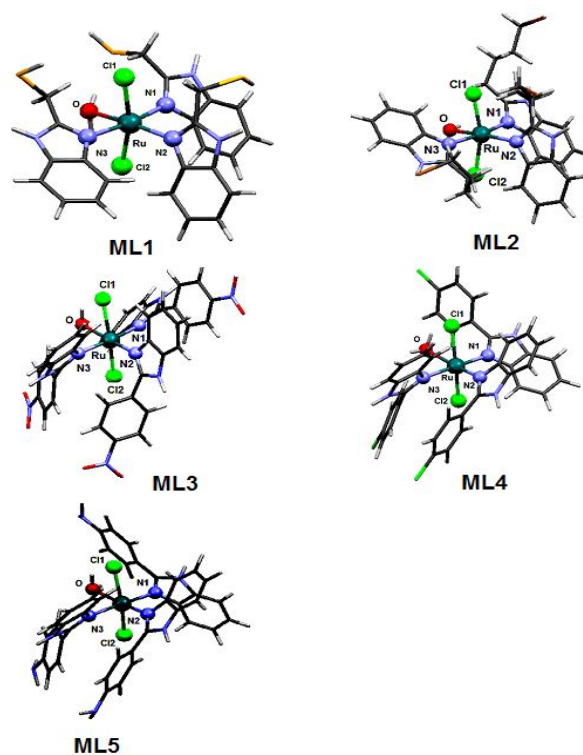


Figure 1: Perspective view of the optimized geometry of metal complexes.

Table1: Pertinent optimized geometrical parameters for the metal complexes (bond length (Å) and bond angle (°)).

Parameters	ML1	ML2	ML3	ML4	ML5
Ru-N1	2.191	2.222	2.161	2.194	2.225
Ru-N2	2.208	2.276	2.207	2.141	2.154
Ru-N3	2.244	2.233	2.278	2.200	2.187
Ru-Cl1	2.540	2.505	2.456	2.559	2.555
Ru-Cl2	2.530	2.560	2.584	2.473	2.483
Ru-O	2.247	2.238	2.240	2.295	2.229
Cl1-Ru-Cl2	167.02	168.60	167.60	165.34	164.43
Cl1-Ru-N1	95.17	94.10	90.45	88.97	93.65
Cl1-Ru-N2	93.78	95.46	90.24	95.49	95.05
Cl1-Ru-N3	81.68	83.63	86.96	92.88	89.34
N2-Ru-N1	86.63	88.61	88.31	92.00	93.00
Cl2-Ru-N1	89.75	62.00	93.66	83.35	81.99
Cl2-Ru-N2	98.51	99.90	101.49	97.24	100.08
Cl2-Ru-N3	81.68	87.65	86.84	94.38	94.72

Biological activities:

Cell viability and cellular morphology study: The cellular morphological alterations at 10, 20, 40, 80 and 160 μM concentrations of complexes were observed under inverted phase contrast microscope after 24 h in THP-1 cells Figure 2-6 (A, B, C, D and E). All complexes treated THP-1 cells showed typical morphological feature of apoptosis viz. cellular shrinkage, nuclear fragmentation and condensation as compared to the untreated cells suggested cellular apoptosis.³² The MTT assay showed that all synthesized complexes significantly ($p < 0.001$) induce the anti-proliferative and cytotoxicity effects on THP-1 cells after 24h exposure Figure 6.

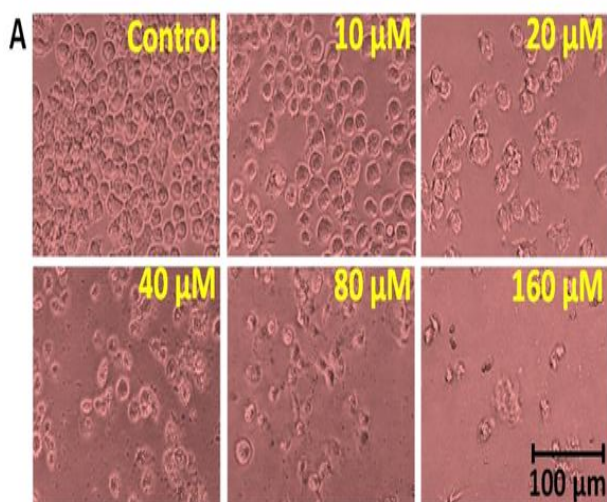


Figure 2: Cellular alterations showing anti-proliferative effect of compound ML2 in THP-1 cells of human acute monocytic leukemia.

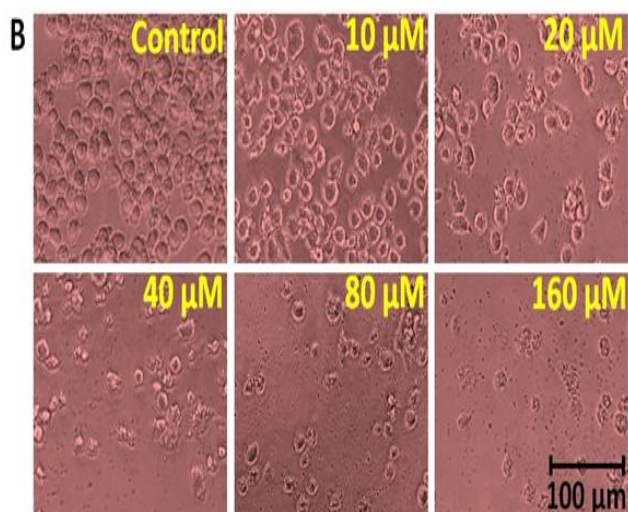


Figure 3: Cellular alterations showing anti-proliferative effect of compound ML4 in THP-1 cells of human acute monocytic leukemia.

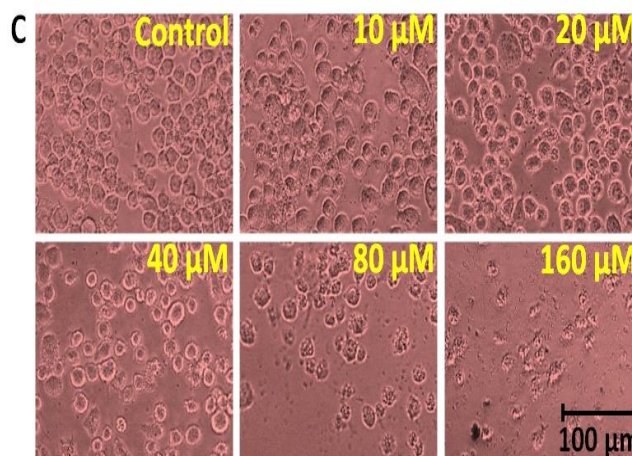


Figure 4: Cellular alterations showing anti-proliferative effect of compound ML5 in THP-1 cells of human acute monocytic leukemia.

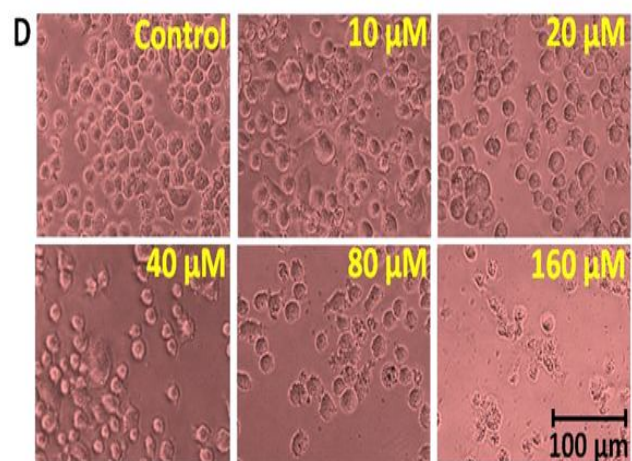


Figure 5: Cellular alterations showing anti-proliferative effect of compound ML3 in THP-1 cells of human acute monocytic leukemia.

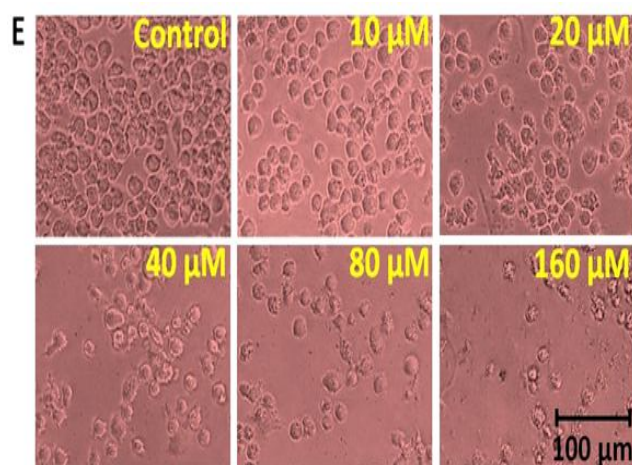


Figure 6: Cellular alterations showing anti-proliferative effect of compound ML1 in THP-1 cells of human acute monocytic leukemia.

Cell viability data revealed that ML4 encourages highest cytotoxicity and reduced the cell viability of THP-1 cells at 10, 20, 40, 80 and 160 μM concentrations about 83.34, 66.74, 59.28, 48.37 and 38.37%, respectively followed by ML2 at the same concentrations reduces the cell viability approximately 85.74, 70.98, 62.59, 51.89 and 39.97% as compared to control cells. Likewise, HL5, HL3 and ML1 reduces the cell viability of THP-1 cells and the sequence of cytotoxicity was ML4 > ML2 > HL5 > ML3 > ML1. The findings revealed that the synthesized complexes significantly reduced the viability of human monocytic leukemia THP-1 cells in a concentration-dependent manner.

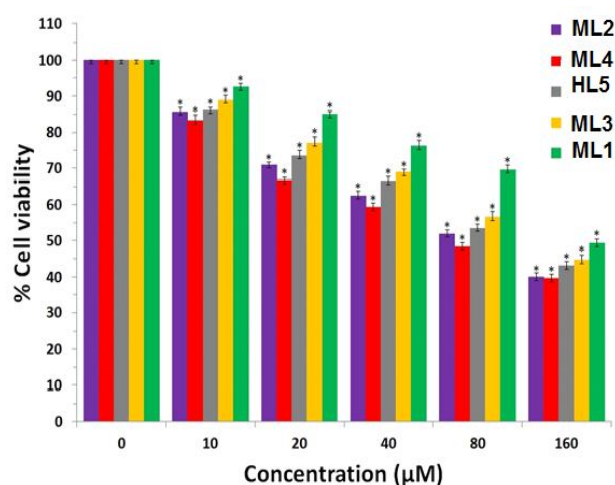


Figure 7: The percent cell viability of THP-1 cells was measured after the exposure of compounds A, B, C, D and E by MTT assay. The three independent experiments were performed and the values are represented as means \pm SEM as compared with the control.

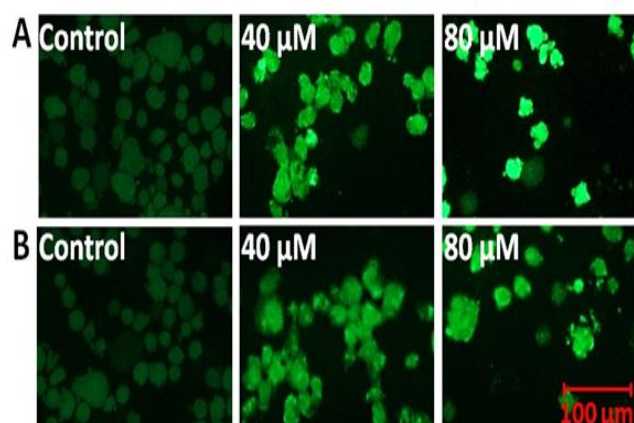


Figure 8: Photomicrograph representing the intracellular ROS production of ML4 and ML2 at 40 and 80 μM concentrations on THP-1 cells of human acute monocytic leukemia.

Intracellular ROS production: The synthesized complexes ML4 and ML2 significantly induce the ROS-mediated cellular apoptosis in THP-1 cells as compared to control cells (Figure 8 A and B). The quantitative DCF fluorescence data revealed that ML4 at 40 and 80 μM concentrations induced 129.91 and 141.99 % (*** $p < 0.001$), respectively as compared to untreated THP-1 cells. Whereas, ML2 induced 117.86% and 132.74% ROS enhancement at 40 and 80 μM concentrations (Figure 8). The findings revealed that both complexes significantly enhance the ROS mediated cell death in human monocytic leukemia THP-1 cells.

Nuclear fragmentation: The nuclear fragmentation analysis exposed that both synthesized complexes ML4 and ML2 significantly encourages nuclear fragmentation and condensation of THP-1 cells in a dose-dependent manner (Figure 9).

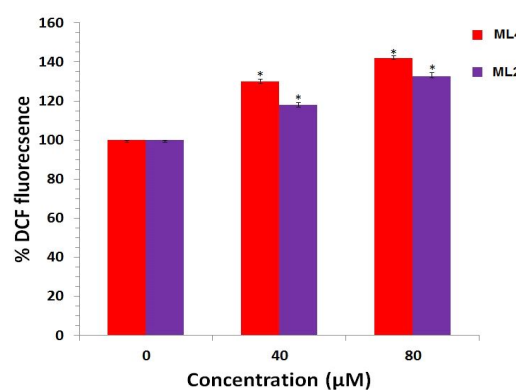


Figure 9: Graph representing %DCF fluorescence at 40 and 80 μM concentrations of ML4 and ML2 against THP-1 cells as compared to the control cells. Data were represented as Mean \pm SEM of three independent experiments and value of $p^{***} \leq 0.001$.

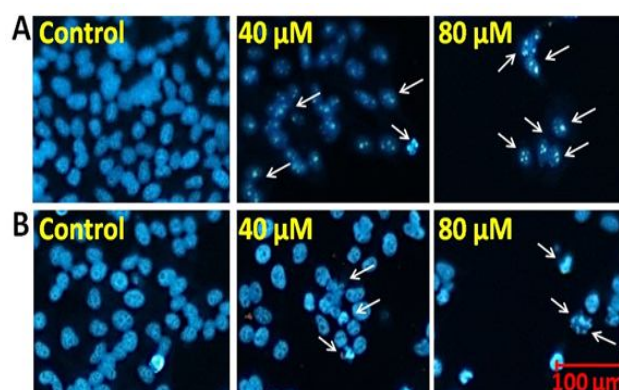


Figure 10: Photomicrograph showing morphological changes, nuclear condensation and cellular apoptosis on THP-1 cells, treated with 40 and 80 μM concentrations of ML4 and ML2.

The morphological alterations by fluorescence nuclear dye DAPI showed condensation in nuclear chromatin and fragmented apoptotic cells, suggests nuclear apoptotic death in THP-1 cells as compared to control. As evident from the quantitative graph representing % apoptotic cells induced by ML4 showed approximately 19.33 and 25.66% apoptotic cells in THP-1 cells at 40 and 80 μM concentrations. While, at 40 and 80 μM concentrations of ML2, showed around 11.67 and 15.33 % of apoptotic cells with respect to the control (Figure 10). The quantitative apoptotic cells analysis and the photomicrograph of THP-1 cells having condensed and fragmented nucleus suggest that both complexes induced the nuclear cell death. The cellular morphological alterations and MTT assay suggested that these synthesized complexes significantly reduced the THP-1 cells viability in a concentration-dependent manner. The accumulation of ROS production and increased number of fragmented nuclei, also suggested that both synthesized complexes ML4 and ML2 induced apoptotic cell death in THP-1 cells of

human acute monocytic leukemia in a dose-dependent manner.

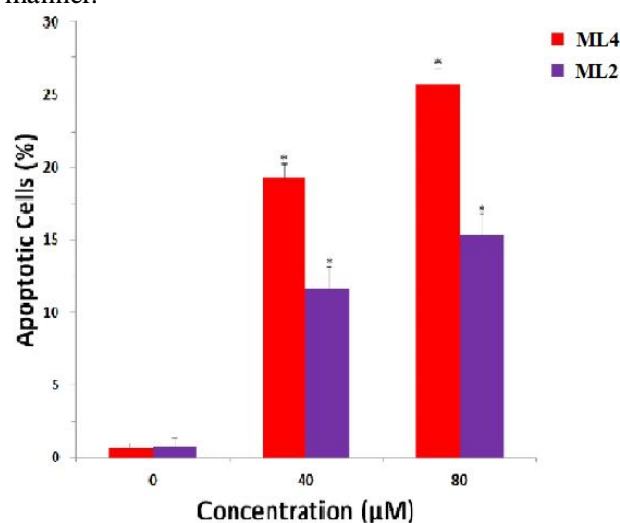


Figure 11: Graph representing % apoptotic cells in THP-1 cells at 40 and 80 μM concentrations of ML4 and ML2.

Table 2: The percentage cell viability of the complexes at different concentrations. Data were represented as Mean \pm SEM of three independent experiments and value of $p^{***} \leq 0.001$.

S. No.	Conc. (in $\mu\text{g/ml}$)	ML2 (% cell viability)	ML4 (% cell viability)	ML5 (% cell viability)	ML3 (% cell viability)	ML1 (% cell viability)
1	0	100	100	100	100	100
2	10	85.74	83.34	86.18	88.92	92.63
3	20	70.98	66.74	73.61	77.13	85.15
4	40	62.59	59.28	66.56	68.91	76.20
5	80	51.89	48.37	53.49	56.53	69.65
6	160	39.97	38.67	43.15	44.75	49.23

CONCLUSION: In conclusion five benzimidazole (HL1-HL5) and their corresponding ruthenium complexes (ML1-ML5) have been synthesised and characterised by physico-chemical methods. The molecular geometry of metal complexes has been optimised by Gaussian-09. The in vitro cytotoxicity studies of all the compounds has been evaluated against the THP-1 cells of human acute monocytic leukemia and compared to cisplatin, oxaliplatin and carboplatin. The benzimidazole exhibited lower antiproliferative activities but the complexes were found to exhibit moderate activities.

ACKNOWLEDGEMENT: We gratefully acknowledge Rajiv Gandhi National Fellowship for financial Support.

REFERENCES:

- Govender P., Renfrew A. K., Clavel C. M., Dyson P. J. (2011) Antiproliferative activity of chelating N,O- and N,N-ruthenium(II) arene functionalised poly(propyleneimine) dendrimer scaffolds, *Dalton Trans.*, 40, 1158–1167.
- Yan Y. K., Melchart M., Habtemariam A., Sadler P. J. (2005) Organometallic chemistry, biology and medicine: ruthenium arene anticancer complexes, *Chem. Commun.*, 38, 4764–4776.
- Melchart M., Habtemariam A., Parsons S., Mogach S. A., Sadler P. J. (2006) Ruthenium(II) arene complexes containing four- and five-membered monoanionic O,O-chelate rings, *Inorganica Chim. Acta.*, 359, 3020–3028.

4. Rajapakse S. K., Martinez A., Naoulou B., Jarzecki A. A. (2009) Ruthenium(II) arene complexes containing four- and five-membered monoanionic O,O chelaterings, *Inorg. Chem. Front.*, 48, 1122–1131.
5. Ochocki J., Kasprzak M., Checinska L. (2010) Properties and applications of flavonoid metal complexes, *Dalton Trans.*, 39, 9711–9718.
6. Clarke M. J. (2003) Ruthenium metallopharmaceuticals, *Coord. Chem. Rev.*, 236, 209–233.
7. Alpan A. S., Zencir S., Zupko I. (2009) Biological activity of bis-benzimidazole derivatives on DNA topoisomerase I and HeLa, MCF7 and A431 cells, *J Enzym Inhib Med Ch.*, 24(3), 844–849.
8. Thota S., Rodrigues D. A., Debbie C. (2018) Crans, Ru(II) Compounds: Next-Generation Anticancer Metallotherpicks, *J. Med. Chem.*, 61, 5805–5821.
9. Sullivan B. P., Meyer T. J. (1982) Comparisons of the physical and chemical properties of isomeric pairs.2. Photochemical, thermal and electrochemical cis-trans isomerizations of $M(\text{Ph}_2\text{PCH}_2\text{PPh}_2)_2\text{Cl}_2$ ($M = \text{Ru(II)}, \text{Os(II)}$), *Inorg. Chem.*, 21, 1037-1040.
10. Lazarevi T., Ana Rilak A., Zivadin D. Bugarcic Z. D. (2017) Platinum, palladium, gold and ruthenium complexes as anticancer agents: Current clinical uses, cytotoxicity studies and future perspectives, *Eur. J. Med. Chem.*, 142, 8-31.
11. Allardyce C. S. and Dyson P. J. (2001) Ruthenium in Medicine: Current Clinical Uses and Future Prospects, *Platin Met Rev.*, 45(2), 62.
12. P. J. Hay, W. R. Wadt (1985) Ab initio effective core potentials for molecular calculations. Potentials for the transition metal atoms Sc to Hg, *J. Chem. Phys.*, 82, 299.
13. Bard A. J., Faulkner L.R. (1990) *Electrochemical methods: fundamentals and applications*, Wiley, New York, pp 864.
14. Wang Y. M., Liu W., Yin X. B. (2017) The development of anticancer ruthenium (II) complexes: from single molecule compounds to nanomaterials, *Chem Soc Rev.*, 8, 3891–3897.
15. Gianferrara T., Bratsos I., Alessio E. (2009) A categorization of metal anticancer compounds based on their mode of action, *Dalton Trans.*, 37, 7588–7598.
16. Vock C., Scolaro C., Phillips A. D. (2006) Synthesis, Characterization, and in Vitro Evaluation of Novel Ruthenium(II) η^6 -Arene Imidazole Complexes, *J Med Chem.*, 49, 5552–5561.
17. Sava G, Bergamo A., Anticancer. Res. (1999) Primary Tumor, Lung and Kidney Retention and Antimetastasis Effect of NAMI-A Following Different Routes of Administration, *Invest. New Drug*, 19, 1117.
18. Balendiran G. K., Dabur R., Fraser D. (2004) Role of Glutathione in Cancer Progression and Chemoresistance, *Biochem.Funct*, 22(6), 343-52.
19. Wong E., Giandomenico C. M. (1999) Current Status of Platinum-Based Antitumor, Drugs *Chemical Reviews*, 99(9), 2451-66.
20. Zamble D. B., Lippard S. J. (1995) Cisplatin and DNA repair in cancer chemotherapy, *Trends in Biochemical Sciences*, 20(10), 435-9.
21. Ang W. H., Dyson P. J. (2006) Classical and Non-Classical Ruthenium-Based Anticancer Drugs: Towards Targeted Chemotherapy, *Euro-pian Inorg Chem.*, 20, 4003-4018.
22. Thota, S. Karki S., Jayaveera K. N., Balzarini (2010) Synthesis, characterization, antitumor, and cytotoxic activity of mononuclear Ru (II) complexes, *J. Coordin.Chem*, 63(24), 4332-4346.
23. Bilakhiya A. K., Tyagi B., Paul P. (2002) Designing Dendrimers Based on Transition-Metal Complexes. Light-Harvesting Properties and Predetermined Redox, Patterns, *Inorg. Chem.*, 41(15), 3830-3842.
24. Ding W. Q., Liu B., Vaught J. L. (2005) Clioquinol and docosahexaenoic acid act synergistically to kill tumor cells, *Cancer Res.*, 65(8), 3389-95.
25. Sun D., Zhang W. & Yang E. (2015) Investigation of antibacterial activity and related mechanism of a ruthenium(II) polypyridyl complex, *Inorg Chem Commun.*, 56, 17–21.
26. Grushin V. V. (2004) Mixed Phosphine-Phosphine Oxide Ligands, *Chem Rev.*, 104, 1629–1662.
27. Kathirvelan D., Yuvaraj P., Babu K., Nagarajan A.S. & Reddy S. R. (2013) A green synthesis of benzimidazoles, *Indian J Chem B*, 52B, 1152-1156.
28. Thangadurai T. D., Gowri M., and Natarajan K. (2002) Synthesis and Characterisation of Ruthenium(II) Complexes Containing Monobasic Bidentate Schiffbases And Their Biological Activities, *Synth React Inorg Met Org Chem.*, 32(2), 329–343 .
29. Roopashree B., Gayathri V. A. Gopi A. & Devaraju K. S. (2012) Syntheses, characterizations, and antimicrobial activities of binuclear ruthenium(III) complexes containing 2-substituted benzimidazole derivatives, *J Coord. Chem.*, 65(22), 4023–4040.
30. Bhattacharyya S., Purkait K. and Mukherjee A. (2017) Ruthenium(II)-p-cymene complexes of abenzimidazole-based ligand capable of VEGFR2

- inhibition: hydrolysis, reactivity and cytotoxicity studies, *Dalton Trans.*, 46, 8539-8554.
31. Mansour A. M., and Shehab O. R. (2017) Photoactivatable CO releasing properties of {Ru(CO)₂}-core pyridylbenzimidazole complexes and reactivity towards Lysozyme, *Inorg. Chem.*, 37, 4299-4310.
32. Pantić D. N., Ljiljana E. Mihajlovic-Lalic L. E. (2019) Synthesis, characterization and cytotoxic activity of organoruthenium(II)-halido complexes with 5-chloro-1H-benzimidazole-2-carboxylic acid, *J. Coord. Chem.*, 72, 908-919.